Diketopyrrolopyrrole (DPP)-Based Donor–Acceptor Polymers for Selective Dispersion of Large-Diameter Semiconducting Carbon Nanotubes

Ting Lei, Ying-Chih Lai, Guosong Hong, Huiliang Wang, Pascal Hayoz, R. Thomas Weitz, Changxin Chen, Hongjie Dai, and Zhenan Bao**

Low-bandgap diketopyrrolopyrrole (DPP)-based polymers are used for the selective dispersion of semiconducting single-walled carbon nanotubes (s-SWCNTs). Through rational molecular design to tune the polymer–SWCNT interactions, highly selective dispersions of s-SWCNTs with diameters mainly around 1.5 nm are achieved. The influences of the polymer alkyl side-chain substitution (i.e., branched vs linear side chains) on the dispersing yield and selectivity of s-SWCNTs are investigated. Introducing linear alkyl side chains allows increased polymer–SWCNT interactions through close π–π stacking and improved C–H–π interactions. This work demonstrates that polymer side-chain engineering is an effective method to modulate the polymer–SWCNT interactions and thereby affecting both critical parameters in dispersing yield and selectivity. Using these sorted s-SWCNTs, high-performance SWCNT network thin-film transistors are fabricated. The solution-deposited s-SWCNT transistors yield simultaneously high mobilities of 41.2 $cm^2 V^{-1} s^{-1}$ and high on/off ratios of greater than 10^4. In summary, low-bandgap DPP donor–acceptor polymers are a promising class of polymers for selective dispersion of large-diameter s-SWCNTs.

Dr. T. Lei, Dr. Y.-C. Lai, Dr. H. Wang, Prof. Z. Bao
Department of Chemical Engineering
Department of Materials Science and Engineering
Stanford University
Stanford, CA 94305, USA
E-mail: zbao@stanford.edu
Dr. Y.-C. Lai
Graduate Institute of Electronics Engineering
National Taiwan University
Taipei 10617, Taiwan, Republic of China
Dr. G. Hong, Dr. C. Chen, Prof. H. Dai
Department of Chemistry
Stanford University
Stanford, CA 94305, USA
Dr. P. Hayoz
BASF Schweiz AG, GVE/B
Schwarzwaldallee 215, 4002 Basel, Switzerland
Dr. R. T. Weitz
BASF SE, GVE/F
Carl-Bosch-Strasse 38, 67056 Ludwigshafen, Germany
E-mail: thomas.weitz@basf.com

DOI: 10.1002/smll.201403761

1. Introduction

Single-walled carbon nanotubes (SWCNTs) have unique mechanical, chemical, electronic, and optical properties,[1] making them promising candidates for various applications, such as bio/chemical sensors,[2] photovoltaics,[3] flexible electronics,[4] and transparent electrodes.[5] Unfortunately, current large-scale growth methods for SWCNTs produce a mixture of nanotube species with both semiconducting (s-) and metallic (m-) SWCNTs. A number of applications for SWCNTs, such as solar cells, field-effect transistors (FETs), and integrated circuits, specifically require s-SWCNTs with minimal m-SWCNT impurities.[6] Although several post-growth separation methods have been developed, e.g., density gradient ultracentrifugation (DGU),[7] column chromatography,[8] and dielectrophoresis,[9] these methods are either time-consuming or not easily scalable.[10]

Selective dispersion of SWCNTs using conjugated polymers has emerged as a powerful and scalable strategy for enriching s-SWCNTs, since it enables fast separation, high concentration dispersion, fine tuning of the dispersing

properties, as well as promising applications of polymer/SWCNT hybrid materials.[11] Currently, conjugated polymers used for selective dispersion of SWCNTs are mainly large bandgap polymers, such as polythiophene, polyfluorene, and polycarbazole.[12] Scalable purification and enrichment processes have been demonstrated for dispersing small-diameter SWCNTs.[12d,13] Compared with small-diameter s-SWCNTs (<1.3 nm), large-diameter s-SWCNTs are highly desired for electronic devices, because they have higher charge carrier mobility and smaller Schottky barrier.[14] Although several reports showed that conventional conjugated polymers can disperse large-diameter s-SWCNTs, these polymers mainly disperse 1.3 nm s-SWCNTs with a weak dispersion ability for s-SWCNTs with diameters around 1.5 nm.[15] Thus, selective dispersing larger diameter s-SWCNTs is still challenging. Moreover, systematic structure-property relationship understanding for polymer design for selective dispersion of s-SWCNTs remains limited.[12d] In particular, the role of branched versus linear side chains on SWCNT sorting has not been investigated.

Donor–acceptor (D–A) conjugated polymers have been shown in recent years to significantly improve the device performance in polymer-based FETs and photovoltaics.[16] FET mobilities over 10 $cm^2\ V^{-1}\ s^{-1}$ and solar cell power-conversion efficiencies over 10% have been reported using this class of polymers.[17] Compared to traditional large bandgap polymers, low bandgap D–A conjugated polymers usually have planar conjugated units, strong π–π interactions, readily tunable frontier orbital energy levels, high carrier mobility and broad absorption spectra,[18] thereby providing a new class of polymers for selective dispersion of s-SWCNTs and applications of polymer/SWCNT hybrid materials. Importantly, the planar conjugated backbone may allow the polymers to potentially more efficiently wrap around large-diameter low-curvature tubes.

In this work, low bandgap diketopyrrolopyrrole (DPP)-based D–A polymers are used to selectively disperse SWCNTs for the first time. We designed and synthesized four DPP-based D–A conjugated polymers with one identical backbone but various ratios of branched and linear alkyl side chains (**Figure 1**). We hypothesized that introducing linear alkyl chains could significantly improve the polymer and SWCNT interactions and provide better dispersion yield and selectivity for s-SWCNTs. Among the polymers tested, PDPP3T-10 with 10 mol% linear alkyl chains exhibited the best dispersion yield and selectivity. Significantly, these polymers can disperse a large ratio of s-SWCNTs with diameters mainly around 1.5 nm with high purity and SWCNT length in the range of 1–3 μm. Thin-film transistors based on the sorted s-SWCNT random networks simultaneously demonstrate a high mobility of 41.2 $cm^2\ V^{-1}\ s^{-1}$ and on/off ratio of 3.6×10^4. To explain the observed side-chain effects on dispersion yield and selectivity of the DPP polymers, we have also proposed a mechanism for the selective dispersion of s-SWCNTs.

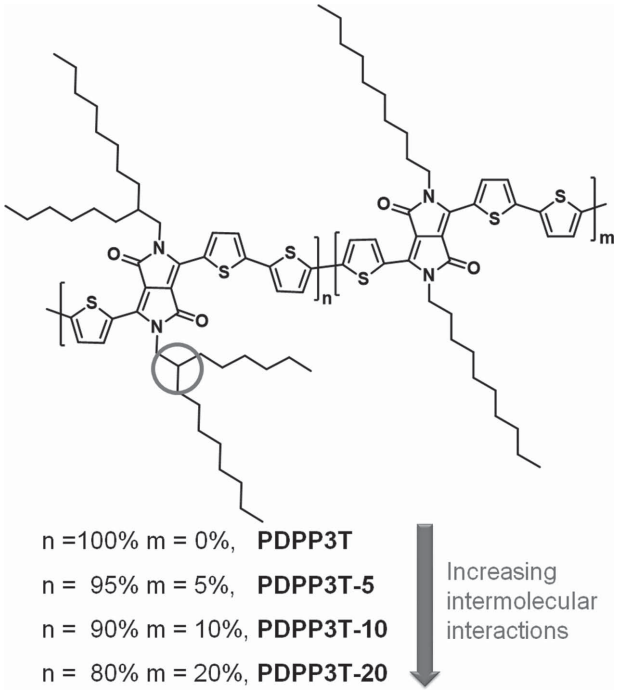

Figure 1. Molecular structures of the four DPP-based conjugated polymers. The circle indicates the steric hindrance caused by the branched alkyl chains when polymers interact with SWCNTs.

2. Results

2.1. Molecular Design, Synthesis, and Polymer Properties

DPP-based polymers are identified because of their strong intermolecular interactions and high reported transistor mobilities.[16c] To guarantee good solubility in such polymers, branched alkyl chains are usually used. The role of alkyl side chains is mainly to serve as solubilizing groups; however, recent studies suggest that side chains of conjugated polymers have substantial impact on the physical properties, molecular packing, and charge transport of organic materials.[19] For example, branched alkyl chains may hinder close intermolecular π–π stacking depending on the location of the branching point.[20] As such, we systematically introduced various ratios of linear alkyl chains to the polymer backbone in order to reduce the steric hindrance of branched alkyl chains and increase the interactions between polymers and SWCNTs (Figure 1). The synthesis of the four polymers is described in the Supporting Information. All polymers showed excellent thermal stability with decomposition temperature over 390 °C (Figure S1, Supporting Information).

Figure 2a displays the absorption spectra of the four DPP polymers in dilute solution (1×10^{-5} M in toluene). All the polymers showed similar dual-band absorption features (Band I: 500–900 nm, Band II: 350–500 nm) with low bandgaps around 1.36 eV. Band I region is typically attributed to charge-transfer absorption from the donor unit to the DPP unit. After introducing linear alkyl chains, the absorption spectra showed slightly redshift with increased 0–0 and decreased 0–1 vibrational peaks.[21] Moreover, the thin-film absorption spectra of these polymers only showed a very small redshift compared with those in solution (Figure S2, Supporting Information). The absence of the bathochromic effects

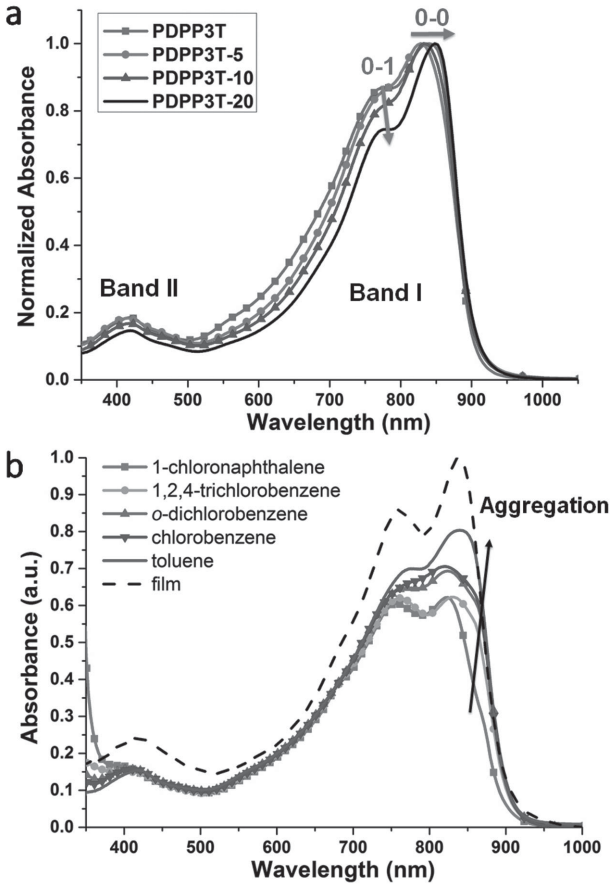

Figure 2. Photophysical properties of the DPP polymers. a) Normalized absorption spectra of four polymers in toluene (1.0×10^{-5} M). b) Absorption spectra of PDPP3T in various solvents (1.0×10^{-5} M) and in thin film format. The film spectra was normalized to the strongest absorption peak.

indicates that some of the polymers formed aggregates in toluene.[22] To test this hypothesis, we measured the absorption spectra of PDPP3T dissolved in a variety of solvents at a low concentration of 1×10^{-5} M (Figure 2b). In toluene, the absorption spectra are close to that in the solid state. With increasing of the dissolving ability of the solvent (from toluene to 1-chloronaphthalene), the absorption of the polymer exhibited obviously blue-shifted features and weaker intensity in Band I region. Similar solvatochromic behavior was also observed in other low bandgap D–A conjugated polymers with strong interchain interactions.[23] Strong π–π interactions can reduce backbone twisting and result in a planarization of polymer backbone, thereby explaining our observed increase in the 0–0 vibrational peak of the Band I region after introducing linear alkyl chains in dilute solutions. This phenomena is seldom observed in large bandgap polymers, such as polyfluorene and polythiophene based polymers, because the interchain interaction in these polymers are weak and they usually display dissociated polymer chains in dilute solutions. Thus, the introduction of the linear alkyl chains can reduce the steric hindrance of branched alkyl chains and led to increased π–π interactions of polymers. Compared to traditional large bandgap polymers, it is expected that these DPP polymers may have stronger interactions with SWCNTs, and is hence potentially beneficial for high-yield and high-selectivity dispersion of SWCNTs.

2.2. Selective Dispersion with DPP Polymers

Commercially available arc-discharged SWCNTs (AD-SWCNTs) with diameters in the range of 1.1–1.8 nm were used. The dispersion process involves the sonication of a mixture of the polymer and AD-SWCNTs in toluene (30 min) followed by centrifugation (30 min) and supernatant collection. We initially used a polymer/AD-SWCNTs ratio of 5/3 mg in 25 mL toluene to disperse the AD-SWCNTs. The main absorption feature of the SWCNTs corresponding to the second interband transition of s-SWCNTs (S_{22}) is at wavelengths from 900–1250 nm for large-diameter SWCNTs (see Figure S3, Supporting Information, for the full absorption spectrum). All the polymers displayed good dispersion ability toward AD-SWCNTs as shown in **Figure 3**a. The well-resolved peaks of the dispersed SWCNTs indicate that the SWCNTs were well-dispersed by polymers. The absorption spectra showed certain background absorption, which comes from the light scattering of some slightly aggregated polymer-wrapped SWCNTs as well as amorphous carbon. Although the SWCNTs are well wrapped by polymers, certain aggregation cannot be fully excluded.[15d,24] The dispersion ability is different for polymers with different amounts of linear alkyl chains. As the linear alkyl chain ratio increased from 0% to 10%, the amount of dispersed SWCNTs increased using PDPP3T-10 (10% linear alky chain), which exhibited the highest dispersion concentration under this condition. However, as the linear alkyl chain ratio was further increased to 20% in PDPP3T-20, the weakest dispersion ability was found. The amount of dispersed s-SWCNT was even lower than that of PDPP3T without any linear alkyl chains.

The absorption ratios between the first interband transition of m-SWCNTs (M_{11}: from 600 to 800 nm) and the second interband transition of s-SWCNTs (S_{22}: from 800 to 1300 nm) can be used to determine the relative amount of m-SWCNT remaining in the dispersed tubes. Since the M_{11} band overlaps with the absorption of DPP polymers, we have to remove the wrapped polymer before determining the selectivity. All the polymers were completely removed by thermal annealing the drop-cast polymer-SWCNT films at 500 °C under Ar. We confirmed that this annealing method does not show any noticeable change in the metallic and semiconducting ratio (Figures S4 and S5, Supporting Information). We also found that the selectivity toward s-SWCNTs varied for polymers with different ratios of linear alkyl chains. As the ratio of linear alkyl chains increases, the M_{11} absorption band intensity decreases accordingly (Figure 3b). It was observed that PDPP3T-20 with 20% linear alkyl chains gave the best selectivity. Since toluene cannot disperse AD-SWCNTs, these results indicate that the DPP polymers can enable dispersion of both s-SWCNTs and m-SWCNTs, but preferably stabilize the s-SWCNTs in the supernatants after sorting process.

The polymer/SWCNT ratio is another critical factor that affects both the dispersion concentration and selectivity

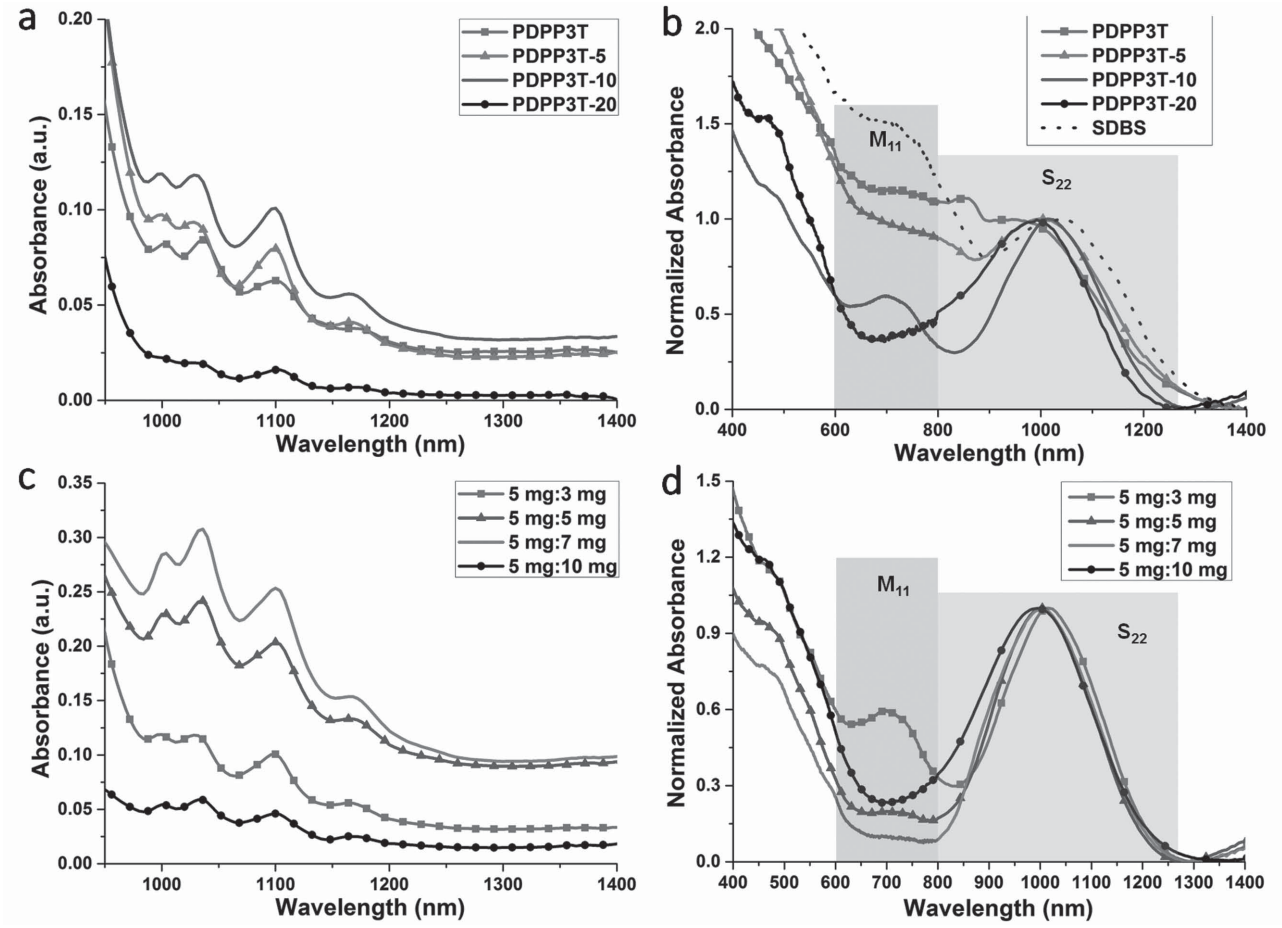

Figure 3. Selective dispersion of s-SWCNTs under different conditions. a) Absorption spectra of AD-SWCNTs dispersed with four DPP polymers at polymer/AD-SWCNT ratio of 5/3 mg. b) Normalized absorption spectra of the polymer-removed sorted SWCNTs and SDBS-removed unsorted SWCNTs in solid state. Samples were prepared by drop-casting the polymer/AD-SWCNT (5/3 mg) solutions or AD-SWCNT 1% SDBS aqueous solution on glass substrate and annealing at 500 °C under Ar for 1 h. c) Absorption spectra of AD-SWCNTs dispersed by PDPP3T-10 with various polymer/AD-SWCNT ratios (5/3 mg, 5/5 mg, 5/7 mg, and 5/10 mg). d) Normalized absorption spectra of the polymer-removed SWCNTs dispersed by PDPP3T-10 with different polymer/AD-SWCNT ratios.

(Figure 3c,d, Figure S6, Supporting Information). Figure 3c,d displays the dispersion concentration and the selectivity of the PDPP3T-10 sorted SWCNTs under various polymer/SWCNT ratios. As the concentration of SWCNTs increased, the amount of the dispersed tubes first increased and then decreased (see Figure S7 (Supporting Information) for details). The decrease in the dispersion amount may be attributed to the absorption of the polymers by the undispersed SWCNT precipitates, which decreased the polymer concentration in solution (Figure S8, Supporting Information). The selectivity showed a similar trend, i.e., selectivity first increased, then decreased as the SWCNT concentration increased (Figure 3d), suggesting that the sorting selectivity is also dependent on the ratio. We observed that PDPP3T-10 showed the highest dispersion yield and satisfactory selectivity at a polymer/SWCNT ratio of 5/7 mg. Under this condition, the estimated yield for sorted s-SWCNT was ≈9% based on the crude AD-SWCNT weight (see the Experimental Section for details). The selectivity of s-SWCNTs under this condition is also high, which is comparable to the commercially available s-SWCNTs (labelled as 99% pure) by DGU method (Figure S9, Supporting Information). Furthermore, compared to either DGU and column chromatography methods that typically require multiple iterations and long purification time (18–24 h) to produce high s-SWCNT enrichment,[7,25] our method can rapidly produce large-diameter s-SWCNT with high yield and high purity within 1 h.

2.3. Raman Characterization of Sorted SWCNTs

To further validate the enrichment of s-SWCNTs, Raman spectra of the pristine AD-SWCNTs, sorted AD-SWCNTs and PDPP3T-10 polymer were measured under three different excitation wavelengths (**Figure 4**). Under the 785 nm excitation, a strong peak at 162 cm^{-1} corresponding to radial breathing modes (RBM) of the metallic tubes was observed in the pristine AD-SWCNTs. After sorting with PDPP3T-10, this peak almost disappeared. Upon excitation via the 633 nm laser, the metallic RBM peak at 200 cm^{-1} disappeared after sorting, whereas the two broad semiconducting peaks at 165 and 230 cm^{-1} still remained. Figure 4c shows *G* peaks under 633 nm excitation. The intensity of G^- peaks of m-SWCNTs at 1500–1550 cm^{-1} obviously decreased, whereas the G^+

www.MaterialsViews.com

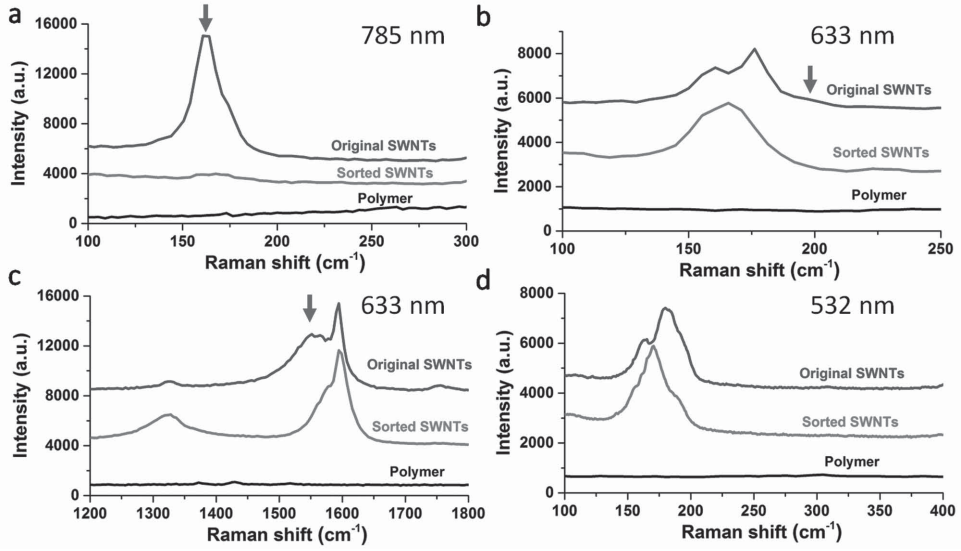

Figure 4. Raman spectra of pristine AD-SWCNTs, AD-SWCNTs sorted by PDPP3T-10, and polymer PDPP3T-10 at different excitation wavelength: a) excited using 785 nm laser, b,c) excited using 633 nm laser, and d) excited using 532 nm laser. The arrows in the spectra indicate the Raman peaks of metallic SWCNTs.

peaks of s-SWCNTs at 1600 cm^{-1} remained unchanged. These results indicate that no significant dispersion of metallic tubes was observed after sorting with PDPP3T-10. Under 532 nm excitation, several RBM peaks of s-SWCNTs were observed in the range of 150–200 cm^{-1} in the pristine AD-SWCNTs. After dispersion and centrifugation, these characteristic peaks remained but their relative intensity have changed, indicating that the employed polymers had preferentially dispersed certain chiralities of s-SWCNTs.

2.4. Chiralities and Diameters of Sorted SWCNTs

To determine the diameters and chiralities of s-SWCNTs dispersed by the DPP polymers, the photoluminescence excitation (PLE) maps of dispersed SWCNTs were measured (**Figure 5**a and Figure S10, Supporting Information). Even though some previous work used UV–Vis-NIR spectrum (S_{11} band) to make the assignments,[15b] the S_{11} peaks of different large-diameter SWCNT species overlap with each other making it difficult to make a precise assignment.[26] Moreover, the dielectric screening by conjugated polymer usually results in shift of the SWCNT absorption wavelength, making the assignments using S_{11} band more difficult.[27] In PLE experiment, s-SWCNTs with both excitation (S_{22}) from 900 to 1010 nm and emission (S_{11}) from 1550 to 2000 nm were measured. We tentatively assign several strong peaks according to the theoretical prediction of the excitation and emission peak positions.[26] A systematic redshift of the peaks was observed, which has been previously reported for polythiophene dispersed SWCNTs and was attributed to dielectric screening caused by the interaction between the polymer and SWCNTs.[27] According to the PLE results, a chiral angle (θ) versus diameter ($\emptyset$) ($\theta/\emptyset$) map is generated from the data sets to visualize the composition of the dispersed SWCNTs (Figure 5b). As indicated by the $\theta/\emptyset$ map, the dominant s-SWCNTs dispersed with PDPP3T-10 were (12, 10) (1.515 nm), (13, 9) (1.521 nm), (13, 8) (1.457 nm), and (14, 7) (1.470 nm), in which the diameters of the dispersed s-SWCNTs are all around 1.5 nm. Note that s-SWCNTs with diameters over 1.6 nm, such as (15, 8) and (20, 1), are also dispersed, demonstrating the high dispersing ability of DPP-based conjugated polymers toward

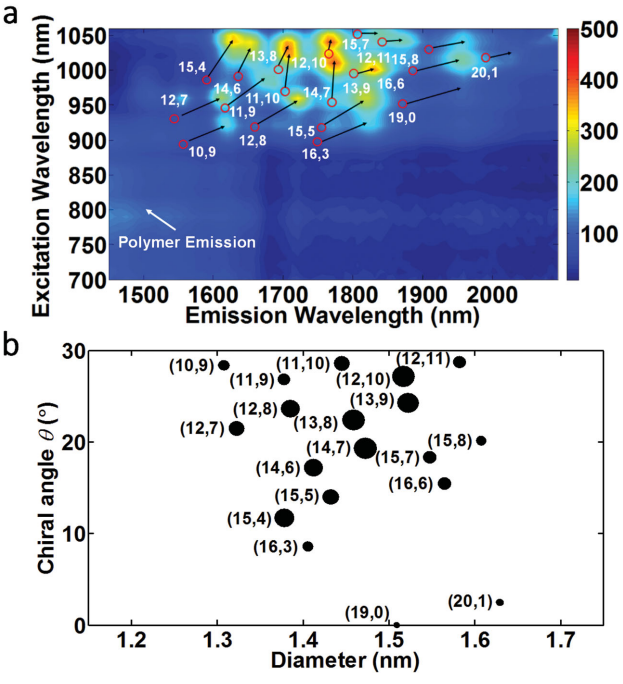

Figure 5. Characterization of the diameters and chiralities of s-SWCNTs dispersed by the DPP polymers. a) PLE maps. The circles indicate theoretical positions of s-SWCNT chiralities as reported by Weisman et al.[26] b) Chiral angle (θ) versus diameter ($\emptyset$) ($\theta/\emptyset$) maps of AD-SWCNTs dispersed in toluene using polymer PDPP3T-10. Within the $\theta/\emptyset$ map, the circle areas are proportional to the concentration of the single species of SWCNTs in the dispersion. The diameters of most s-SWCNTs are in the range from 1.3 to 1.6 nm.

large-diameter SWCNTs. s-SWCNTs dispersed by other DPP polymers with different amounts of linear alkyl chains showed similar chirality distributions as PDPP3T-10 (Figure S10, Supporting Information). We also used poly(3-dodecylthiophene-2,5-diyl) (P3DDT), a polythiophene based polymer for dispersing the same batch of AD-SWCNTs (Figure S11, Supporting Information). The PLE result showed that P3DDT mainly disperse SWCNTs with diameters in the range of 1.3–1.4 nm with a weak dispersion ability of SWCNTs around 1.5 nm. This result demonstrate that the low bandgap DPP D–A polymers tends to disperse larger diameter SWCNTs, probably due to their planar conjugated backbones and strong π–π interactions.

2.5. Thin-film Transistor Characterization of Sorted SWCNTs

To further evaluate the selective sorting of AD-SWCNTs by PDPP3T-10, bottom-gate/bottom-contact (BG/BC) device configuration was used to fabricate SWCNT network thin-film transistors (TFTs). The TFTs were fabricated by soaking the patterned Au (source–drain)/SiO_2 (300 nm)/doped Si substrate in a diluted supernatant for 5 h and then the substrate was rinsed with toluene and annealed at 150 °C for 30 min under ambient conditions. Toluene rinsing was used to remove most of the polymers, which can lead to better tube–tube junctions and improved charge carrier mobility. SWCNT density is a critical parameter for TFT devices based on SWCNT networks.[28] In our method, the performance of the devices can be tuned by soaking the substrates in different concentrations of diluted solutions. **Figure 6**a shows the atomic force microscopy (AFM) height image of a TFT device fabricated by soaking in a 1:10 diluted supernatant solution. Most of the sorted tubes exhibited lengths in the range of 1–3 μm, longer and straighter than previously reported small-diameter SWCNTs.[12d] At a tube density of ≈40 tubes μm^{-2} (Figure 6a), high hole mobilities in the range of 10–17 $cm^2\ V^{-1}\ s^{-1}$ (average: 13.4 ± 1.9 $cm^2\ V^{-1}\ s^{-1}$) with high on/off ratios of 10^5–10^6 were obtained (Figure S12, Supporting Information). A higher tube density of ≈70 tubes μm^{-2} can be obtained by soaking in a 1:5 diluted supernatant (Figure 6b). This condition provided further increased mobility in the range of 15–42 $cm^2\ V^{-1}\ s^{-1}$ (average: 27.6 ± 7.8 $cm^2\ V^{-1}\ s^{-1}$) with on/off ratios of 10^4 to 10^5. Our best transistor demonstrated a high mobility of 41.2 $cm^2\ V^{-1}\ s^{-1}$ and on/off ratio of 3.6×10^4 (Figure 6c,d). The unsorted SWCNT devices with similar tube density have a very low on/off ratios of less than 10, which is attributed to metallic SWCNT pathways.[24] The slightly lowered on/off ratios in comparison with smaller diameter SWCNT (<1.3 nm) networks[12d] are probably due to the low theoretical on/off ratio for large-diameter SWCNTs as a result of the small bandgap.[29] Additionally, these devices were prepared using a simple solution soaking method at low temperature on SiO_2 substrates (without any further surface treatment).[30] Our transistor performances are among the highest for solution-processed random SWCNT network TFTs,[7,12d,15b,24,28,31] and they are surpassing or comparable to some SWCNT network TFTs prepared by chemical vapor deposition (CVD) methods that require high temperature (>800 °C) and vacuum conditions.[4a,32] The observed positive and large threshold voltage are common for SWCNT TFTs measured in air,[12d,33] which is caused by several possibilities: oxygen/water doping or presence of traps.[34] As shown in Figure S14 (Supporting Information), if the device was measured in glove box, the threshold voltage shifted from 30 to 10 V. Furthermore, we are using 300 nm SiO_2 dielectric layer. If a lower thickness SiO_2 or high-k dielectric is used, the operating voltage will be further reduced.

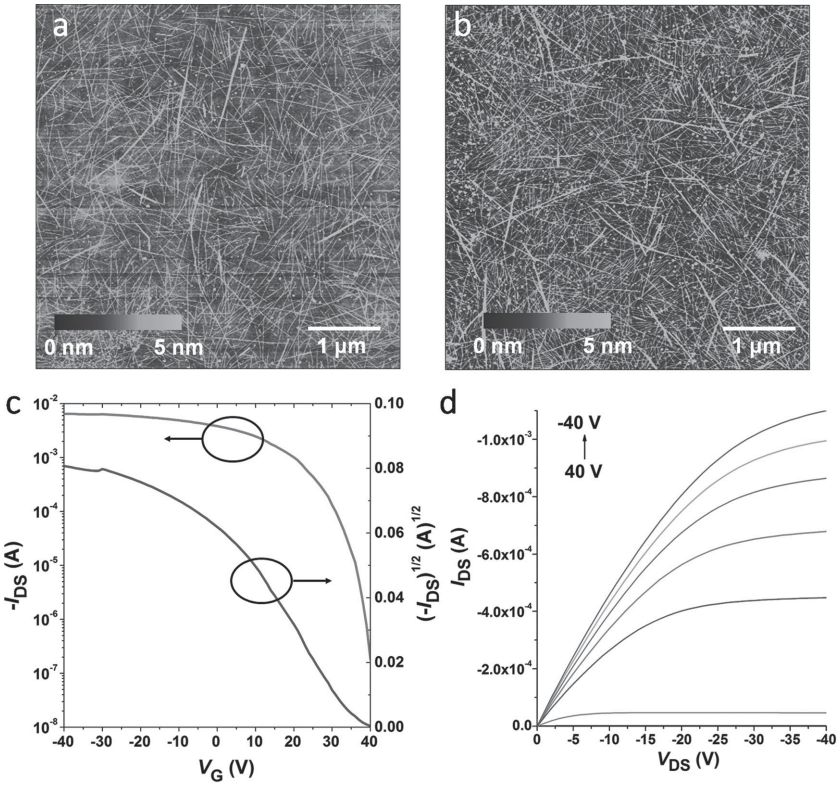

Figure 6. TFT device fabrication and characterization. AFM height images of SWCNT network fabricated by soaking the substrate in a) 1:10 and b) 1:5 diluted supernatant. Higher supernatant concentrations resulted in denser SWCNT networks. c) Transfer and d) output characteristics of a typical TFT device fabricated by soaking in a 1:5 diluted supernatant (L = 100 μm, W = 2000 μm, V_{DS} = −40 V). This transistor demonstrates a high hole mobility of 41.2 $cm^2\ V^{-1}\ s^{-1}$ and an on/off ratio of 3.6×10^4.

3. Discussions

The above results demonstrate that by engineering the alkyl side chains of our employed polymers, we can significantly

affect both the dispersion yield and selectivity. With linear alkyl chains, we observed increased polymer–polymer interactions. This effect is similar to previous observations that branched alkyl chains hinder the close intermolecular π–π stacking (due to their large van der Waals radius near the branching position).[16b] Because the concentrations of the polymer solutions used for SWCNT dispersion were relatively high, ca. 3×10^{-3} M, the polymers were most likely in aggregated states. Polymers with linear side chains have a stronger tendency to aggregate than the branched ones, as indicated from the UV–vis absorption spectra (Figure 2a). Thus, a decreased dispersion would have been expected for polymers with higher linear alkyl chain ratios. On the contrary, we observed that after introducing linear alkyl side-chains up to 10%, the dispersion yield increased instead. This observation indicates a stronger interaction between DPP polymers and SWCNTs with a moderate amount of linear side chains. However, the dispersion ability decreased as the linear side-chain ratio further increased to 20%. We attribute this observation to the following: as the linear side chain ratio increases, the interchain interaction between polymers became stronger than the polymer–SWCNT interaction. As a result, polymers could not break free from the aggregates to disperse SWCNTs. Furthermore, an increasing of the linear alkyl side-chain ratio was observed to give a higher selectivity for s-SWCNTs.

To further understand the effects of alkyl side-chains on polymer/SWCNT interactions, density functional theory (DFT) calculations were performed. The repeating unit of the DPP polymers with linear/branched alkyl chains and s-SWCNTs with chirality of (17, 0) (1.350 nm) and (19, 0) (1.508 nm) were chosen as model systems to represent s-SWCNTs dispersed by our polymers (**Figure 7**). The geometries of the polymer/SWCNT complexes were optimized by the semiempirical method PM7,[35] and the energies of the complexes were calculated using B3LYP-D3 functional using 6–31G(d) as basis set (see the Supporting Information).[36] As shown in Figure 7a,b, our modeling results indicate that DPP units and SWCNT can form stable complexes with π–π stacking distances of ≈3.4 Å and alkyl side chains wrapped on the SWCNT surface through C–H–π interactions.[37] The association energy between a DPP unit with two linear chains and the SWCNT was calculated to be 43.8 kcal mol^{-1} for SWCNT (17, 0), 6.2 kcal mol^{-1} larger than that of the complex formed by DPP with branched chains and SWCNT (Figure 7a,b, and Table S2, Supporting Information). These results agree well with our obtained experimental results that the DPP polymers with low ratios of linear alkyl side chains tend to have stronger dispersion abilities compared to those with only branched side chains. To investigate the contribution from the π–π stacking interactions, we calculated the association energy of the DPP-SWCNT complex by removing the alkyl side-chains, but keeping the coordinates of other atoms unchanged. The π–π stacking interaction under the linear alkyl side-chain geometry is 2.4 kcal mol^{-1} stronger than that of the branched chain geometry, largely attributed to the closer π–π stacking distance of this geometry. We also obtained similar results for SWCNT (19, 0) with a larger diameter (Table S3, Supporting Information).

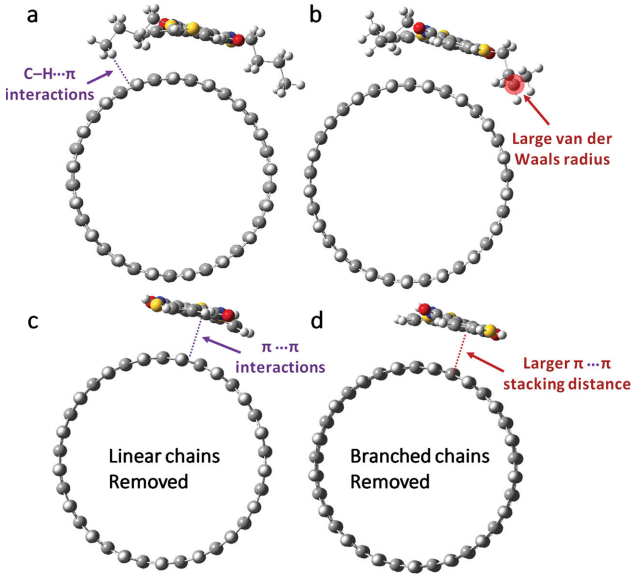

Figure 7. Computational study on the polymer-SWCNT (17, 0) interactions. Optimized geometries of a) DPP unit with linear alkyl chains and b) DPP unit with branched alkyl chains. The long branched chains are replaced by methyl groups to reduce the size of the system, and both DPP units have four carbon alkyl chains. c,d) Molecular models after removing the alkyl side chains, the alkyl chains were replaced by hydrogens. The geometries of c,d) were not reoptimized, in which the coordinates remained the same as a,b), respectively.

Thus, the smaller association energy in the complex formed by SWCNT and DPP unit with branched chains was attributed to both the larger π–π stacking distance and less C–H–π interactions.

In terms of the origin for selective dispersion of s-SWCNTs by conjugated polymers, previous theoretical work suggested a stronger tendency of charge-transfer complex formation between conjugated polymers and m-SWCNTs compared to s-SWCNTs.[38] The charge-transfer complex is expected to be soluble in polar solvents. Indeed, when using polar solvents, e.g., tetrahydrofuran (THF), the amount of m-SWCNT dispersed increases significantly and the DPP polymers did not show any noticeable selectivity (Figure S15, Supporting Information). However, direct evidence proof of the hypothesis remains challenging. On the basis of the charge-transfer complex hypothesis, the selectivity of the DPP polymers with different amounts of linear alkyl chains may be explained as follows: the introduction of linear alkyl side-chains results in a closer π–π stacking and stronger interactions between the DPP polymer and SWCNTs, leading to a stronger charge transfer between conjugated polymers and m-SWCNTs. The stronger charge transfer can induce stronger aggregation tendency of polar m-SWCNT/polymer complex in nonpolar toluene solvent, thereby resulting in higher selectivity toward s-SWCNTs. However, if the ratio of linear side chains is too high, the aggregation between polymers will prevent effective interaction between polymers and SWCNTs, which in turn reduces the amount of SWCNTs dispersed. On the other hand, a better selectivity for s-SWCNTs was observed as a stronger tendency for charge transfer is expected, when more linear side chains are incorporated.

4. Conclusions

In summary, we demonstrate the first example of using low bandgap DPP-based polymers for selective dispersion of s-SWCNTs. Through systematically alkyl side chain engineering, we can modulate the polymer–SWCNT interactions and achieved high-yield and high-selectivity dispersion of s-SWCNTs with diameters mainly around 1.5 nm and some over 1.6 nm. Using DPP-sorted s-SWCNTs, high-performance s-SWCNT network TFTs were fabricated by simple solution processing, and a high mobility of 41.2 $cm^2\ V^{-1}\ s^{-1}$ and an on/off ratio of 3.6×10^4 were demonstrated. Both the yield and selectivity can be tuned by the side-chain engineering of conjugated polymers, which were explained by our proposed mechanism and computational results. In summary, our results demonstrate that low bandgap D–A polymers are a promising class of polymers for the selective dispersion of large-diameter s-SWCNTs.

5. Experimental Section

Preparation of SWCNT Solutions: 5 mg of DPP polymers and 7 mg of arc-discharged SWCNTs (P2 SWCNT, 90% purity for SWCNTs) were mixed in 25 mL of toluene and ultrasonicated for 30 min at an amplitude level of 70% (Cole Parmer ultrasonicator 750 W). The solution was then centrifuged at 17 000 rpm for 30 min at 16 °C (Sorvall RC5C-plus). The supernatant was collected and provided the final sorted s-SWCNT solutions.

To determine the yield for sorted s-SWCNTs, a nylon membrane (0.2 μm pore size) covered with sorted s-SWCNT was prepared by filtering the supernatant through the filter. The nylon membrane was rinsed extensively with hot toluene and chloroform to remove any residue polymer. It was dried under vacuum and the weight was measured to give a 9% yield for PDPP3T-10 sorted s-SWCNTs (5 mg PDPP3T-10 and 7 mg initial AD-SWCNTs). The yield is based on the weight ratio of s-SWCNT and the initial raw AD-SWCNT (90% SWCNTs and 10% amorphous carbons/catalysts).

The dispersion concentration was evaluated by UV–vis-NIR measurements using a 1 cm path-length quartz cells by using a Cary 6000i spectrophotometer (Varian) with toluene as a background. To determine the selectivity, s-SWCNT thin films were prepared by drop-casting the supernatants on glass substrates and annealing the film at 500 °C under Ar for 1 h to remove the wrapped polymers.

Sorted SWCNT Characterization: The Raman spectra (Model: LabRam Aramis from Horiba Jobin Yvon) was carried out at 2.33 eV (532 nm), 1.96 eV (633 nm), and 1.58 eV (785 nm) excitation at ×100 magnification and 1-μm spot size. The peak positions were calibrated with the Si line at 521 cm^{-1}. Polymers were removed by 500 °C annealing under Ar before taking the Raman spectra. The Raman spectra were normalized according to the G peak. All the Raman spectra were taken under the same conditions. AFM studies were performed with a NanoScope IV microscope, and all experiments were carried out in tapping mode under ambient conditions. A silicon nitride cantilever was used with a resonant frequency around 300 kHz.

The PLE spectra of various SWCNT samples in toluene were taken on a home-built NIR-II spectroscopy setup with measured range of 1100–2100 nm. The excitation in the 700–1080 nm range was provided by a white-light source of an ozone-free Hg/Xe lamp (Oriel) with a total output power of 200 W. The lamp illumination was filtered by an UV filter (Thorlabs) to remove the ultraviolet light, and an 1100 nm short-pass filter (Omega) to remove the NIR-II light with wavelengths longer than 1100 nm. The excitation light cleaned by these filters was dispersed by a grating-based monochromator (Oriel), generating excitation lines at a single, user-designated wavelength with a bandwidth of 15 nm. The monochromatic excitation light was then focused onto a 1 mm path quartz cuvette (Starna Cells) with the SWCNT solution loaded inside. The emitted fluorescence from the SWCNT solution was collected in the transmission geometry, where the transmitted excitation light was rejected by an 1100-nm long-pass filter (Thorlabs). Fluorescence in the range of 1100–2100 nm was allowed to pass through the emission filter and was collected by a grating-based triple-turret spectrometer (Acton SP2300i) equipped with a 1D indium–gallium–arsenide (InGaAs) linear array detector (Princeton Instruments 1D OMA-V). The raw PLE spectra were corrected after data acquisition, in order to account for the difference of excitation power at different wavelengths, the extinction profile of the emission filter, and the sensitivity profile of the 1D detector, using the MATLAB software.

TFT Fabrication and Characterization: The drain and source electrodes for bottom-contact device electrodes were fabricated on a highly doped 4 in. silicon wafer with 300 nm SiO_2 by photolithography. A bilayer of Cr (3 nm) and Au (25 nm) was deposited by thermal evaporation as the source–drain electrodes, followed by a lift-off process in acetone. The substrate was soaked in the diluted solution of sorted SWCNTs (1:5 ratio in toluene) for 5 h, and then was rinsed with toluene, dried with nitrogen flow, and annealed at 150 °C for 30 min under ambient conditions. The evaluations of the FETs were carried out in atmosphere on a probe stage using a Keithley 4200 SCS as parameter analyzer. The carrier mobility, μ, was calculated from the data in the saturated regime according to the equation $I_{SD} = (W/2L)C_i\mu(V_G - V_T)^2$, where I_{SD} is the drain current in the saturated regime. W and L are the semiconductor channel width and length. C_i is the parallel plate capacitance of 300 nm SiO_2 (11 nF cm^{-2}). V_G and V_T are the gate voltage and threshold voltage, respectively. $V_G - V_T$ of the device was determined from the relationship between the square root of I_{SD} and V_G at the saturated regime.

Supporting Information

Supporting Information is available from the Wiley Online Library or from the author.

Acknowledgements

We thank Igor Porchorovski, Steve Park, and Jeffrey B.-H. Tok for discussion. Y.C.L. thanks his supporting funding from Taiwan National Science Council (102-2917-i-002-087).

[1] a) P. J. F. Harris, *Carbon Nanotube Science: Synthesis, Properties and Applications*, Cambridge University Press, New York, USA, **2011**; b) H. Dai, *Acc. Chem. Res.* **2002**, *35*, 1035.

[2] E. S. Snow, F. K. Perkins, E. J. Houser, S. C. Badescu, T. L. Reinecke, *Science* **2005**, *307*, 1942.
[3] a) M. P. Ramuz, M. Vosgueritchian, P. Wei, C. Wang, Y. Gao, Y. Wu, Y. Chen, Z. Bao, *ACS Nano* **2012**, *6*, 10384; b) R. M. Jain, R. Howden, K. Tvrdy, S. Shimizu, A. J. Hilmer, T. P. McNicholas, K. K. Gleason, M. S. Strano, *Adv. Mater.* **2012**, *24*, 4436; c) Y. Ye, D. J. Bindl, R. M. Jacobberger, M.-Y. Wu, S. S. Roy, M. S. Arnold, *Small* **2014**, *10*, 3299.
[4] a) Q. Cao, H.-s. Kim, N. Pimparkar, J. P. Kulkarni, C. Wang, M. Shim, K. Roy, M. A. Alam, J. A. Rogers, *Nature* **2008**, *454*, 495; b) S. Park, M. Vosguerichian, Z. Bao, *Nanoscale* **2013**, *5*, 1727.
[5] a) H. Gu, T. M. Swager, *Adv. Mater.* **2008**, *20*, 4433; b) D. S. Hecht, L. Hu, G. Irvin, *Adv. Mater.* **2011**, *23*, 1482; c) L. Hu, G. Gruner, J. Gong, C.-J. C. Kim, B. Hornbostel, *Appl. Phys. Lett.* **2007**, *90*, 093124.
[6] a) C. Wang, K. Takei, T. Takahashi, A. Javey, *Chem. Soc. Rev.* **2013**, *42*, 2592; b) M. C. Hersam, *Nat. Nanotechnol.* **2008**, *3*, 387; c) Q. Cao, S.-J. Han, G. S. Tulevski, Y. Zhu, D. D. Lu, W. Haensch, *Nat. Nanotechnol.* **2013**, *8*, 180.
[7] M. S. Arnold, A. A. Green, J. F. Hulvat, S. I. Stupp, M. C. Hersam, *Nat. Nanotechnol.* **2006**, *1*, 60.
[8] Y. Miyata, K. Shiozawa, Y. Asada, Y. Ohno, R. Kitaura, T. Mizutani, H. Shinohara, *Nano Res.* **2011**, *4*, 963.
[9] R. Krupke, F. Hennrich, H. V. Löhneysen, M. M. Kappes, *Science* **2003**, *301*, 344.
[10] H. Zhang, B. Wu, W. Hu, Y. Liu, *Chem. Soc. Rev.* **2011**, *40*, 1324.
[11] a) K. S. Mistry, B. A. Larsen, J. L. Blackburn, *ACS Nano* **2013**, *7*, 2231; b) F. Jakubka, S. P. Schießl, S. Martin, J. M. Englert, F. Hauke, A. Hirsch, J. Zaumseil, *ACS Macro Lett.* **2012**, *1*, 815; c) N. Berton, F. Lemasson, J. Tittmann, N. Stürzl, F. Hennrich, M. M. Kappes, M. Mayor, *Chem. Mater.* **2011**, *23*, 2237; d) L. Qian, W. Xu, X. Fan, C. Wang, J. Zhang, J. Zhao, Z. Cui, *J. Phys. Chem. C* **2013**, *117*, 18243.
[12] a) K. Akazaki, F. Toshimitsu, H. Ozawa, T. Fujigaya, N. Nakashima, *J. Am. Chem. Soc.* **2012**, *134*, 12700; b) N. Berton, F. Lemasson, A. Poschlad, V. Meded, F. Tristram, W. Wenzel, F. Hennrich, M. M. Kappes, M. Mayor, *Small* **2014**, *10*, 360; c) V. Derenskyi, W. Gomulya, J. M. S. Rios, M. Fritsch, N. Fröhlich, S. Jung, S. Allard, S. Z. Bisri, P. Gordiichuk, A. Herrmann, U. Scherf, M. A. Loi, *Adv. Mater.* **2014**, *26*, 5969; d) H. W. Lee, Y. Yoon, S. Park, J. H. Oh, S. Hong, L. S. Liyanage, H. Wang, S. Morishita, N. Patil, Y. J. Park, J. J. Park, A. Spakowitz, G. Galli, F. Gygi, P. H. S. Wong, J. B. H. Tok, J. M. Kim, Z. Bao, *Nat. Commun.* **2011**, *2*, 541.
[13] a) A. Nish, J.-Y. Hwang, J. Doig, R. J. Nicholas, *Nat. Nanotechnol.* **2007**, *2*, 640; b) S. K. Samanta, M. Fritsch, U. Scherf, W. Gomulya, S. Z. Bisri, M. A. Loi, *Acc. Chem. Res.* **2014**, *47*, 2446.
[14] a) X. Zhou, J.-Y. Park, S. Huang, J. Liu, P. L. McEuen, *Phys. Rev. Lett.* **2005**, *95*, 146805; b) Z. Chen, J. Appenzeller, J. Knoch, Y.-m. Lin, P. Avouris, *Nano Lett.* **2005**, *5*, 1497.
[15] a) M. Tange, T. Okazaki, S. Iijima, *J. Am. Chem. Soc.* **2011**, *133*, 11908; b) W. Gomulya, G. D. Costanzo, E. J. F. de Carvalho, S. Z. Bisri, V. Derenskyi, M. Fritsch, N. Fröhlich, S. Allard, P. Gordiichuk, A. Herrmann, S. J. Marrink, M. C. dos Santos, U. Scherf, M. A. Loi, *Adv. Mater.* **2013**, *25*, 2948.
[16] a) S. Holliday, J. E. Donaghey, I. McCulloch, *Chem. Mater.* **2014**, *26*, 647; b) T. Lei, J.-Y. Wang, J. Pei, *Acc. Chem. Res.* **2014**, *47*, 1117; c) C. B. Nielsen, M. Turbiez, I. McCulloch, *Adv. Mater.* **2013**, *25*, 1859.
[17] a) C. Luo, A. K. K. Kyaw, L. A. Perez, S. Patel, M. Wang, B. Grimm, G. C. Bazan, E. J. Kramer, A. J. Heeger, *Nano. Lett.* **2014**, *14*, 2764; b) J. You, L. Dou, K. Yoshimura, T. Kato, K. Ohya, T. Moriarty, K. Emery, C.-C. Chen, J. Gao, G. Li, Y. Yang, *Nat. Commun.* **2013**, *4*, 1446.
[18] J. D. Yuen, F. Wudl, *Energy Environ. Sci.* **2013**, *6*, 392.
[19] a) T. Lei, J.-Y. Wang, J. Pei, *Chem. Mater.* **2014**, *26*, 594; b) J. Mei, Z. Bao, *Chem. Mater.* **2014**, *26*, 604.
[20] a) T. Lei, J.-H. Dou, J. Pei, *Adv. Mater.* **2012**, *24*, 6457; b) J. Mei, D. H. Kim, A. L. Ayzner, M. F. Toney, Z. Bao, *J. Am. Chem. Soc.* **2011**, *133*, 20130.
[21] F. C. Spano, C. Silva, *Annu. Rev. Phys. Chem.* **2014**, *65*, 477.
[22] a) N. Zhou, X. Guo, R. P. Ortiz, S. Li, S. Zhang, R. P. H. Chang, A. Facchetti, T. J. Marks, *Adv. Mater.* **2012**, *24*, 2242; b) T. Lei, J.-H. Dou, X.-Y. Cao, J.-Y. Wang, J. Pei, *J. Am. Chem. Soc.* **2013**, *135*, 12168.
[23] R. Steyrleuthner, M. Schubert, I. Howard, B. Klaumünzer, K. Schilling, Z. Chen, P. Saalfrank, F. Laquai, A. Facchetti, D. Neher, *J. Am. Chem. Soc.* **2012**, *134*, 18303.
[24] H. Wang, J. Mei, P. Liu, K. Schmidt, G. Jiménez-Osés, S. Osuna, L. Fang, C. J. Tassone, A. P. Zoombelt, A. N. Sokolov, K. N. Houk, M. F. Toney, Z. Bao, *ACS Nano* **2013**, *7*, 2659.
[25] G. S. Tulevski, A. D. Franklin, A. Afzali, *ACS Nano* **2013**, *7*, 2971.
[26] R. B. Weisman, S. M. Bachilo, *Nano Lett.* **2003**, *3*, 1235.
[27] O. Kiowski, S. Lebedkin, F. Hennrich, S. Malik, H. Rösner, K. Arnold, C. Sürgers, M. M. Kappes, *Phys. Rev. B* **2007**, *75*, 075421.
[28] T. Takahashi, K. Takei, A. G. Gillies, R. S. Fearing, A. Javey, *Nano Lett.* **2011**, *11*, 5408.
[29] A. Javey, M. Shim, H. Dai, *Appl. Phys. Lett.* **2002**, *80*, 1064.
[30] C. Wang, D. Hwang, Z. Yu, K. Takei, J. Park, T. Chen, B. Ma, A. Javey, *Nat. Mater.* **2013**, *12*, 899.
[31] a) S. Z. Bisri, J. Gao, V. Derenskyi, W. Gomulya, I. Iezhokin, P. Gordiichuk, A. Herrmann, M. A. Loi, *Adv. Mater.* **2012**, *24*, 6147; b) M. C. LeMieux, M. Roberts, S. Barman, Y. W. Jin, J. M. Kim, Z. Bao, *Science* **2008**, *321*, 101; c) H. Okimoto, T. Takenobu, K. Yanagi, Y. Miyata, H. Shimotani, H. Kataura, Y. Iwasa, *Adv. Mater.* **2010**, *22*, 3981; d) G. J. Brady, Y. Joo, S. Singha Roy, P. Gopalan, M. S. Arnold, *Appl. Phys. Lett.* **2014**, *104*, 083107; e) J. Ding, Z. Li, J. Lefebvre, F. Cheng, G. Dubey, S. Zou, P. Finnie, A. Hrdina, L. Scoles, G. P. Lopinski, C. T. Kingston, B. Simard, P. R. L. Malenfant, *Nanoscale* **2014**, *6*, 2328; f) M. Engel, J. P. Small, M. Steiner, M. Freitag, A. A. Green, M. C. Hersam, P. Avouris, *ACS Nano* **2008**, *2*, 2445; g) M. Shimizu, S. Fujii, T. Tanaka, H. Kataura, *J. Phys. Chem. C* **2013**, *117*, 11744.
[32] a) D.-m. Sun, M. Y. Timmermans, Y. Tian, A. G. Nasibulin, E. I. Kauppinen, S. Kishimoto, T. Mizutani, Y. Ohno, *Nat. Nanotechnol.* **2011**, *6*, 156; b) Q. Cao, M. G. Xia, M. Shim, J. A. Rogers, *Adv. Funct. Mater.* **2006**, *16*, 2355; c) E. S. Snow, P. M. Campbell, M. G. Ancona, J. P. Novak, *Appl. Phys. Lett.* **2005**, *86*, 033105.
[33] C. Wang, L. Qian, W. Xu, S. Nie, W. Gu, J. Zhang, J. Zhao, J. Lin, Z. Chen, Z. Cui, *Nanoscale* **2013**, *5*, 4156.
[34] N. M. Dissanayake, Z. Zhong, *Nano Lett.* **2011**, *11*, 286.
[35] J. P. Stewart, *J. Mol. Model.* **2013**, *19*, 1.
[36] S. Grimme, J. Antony, S. Ehrlich, H. Krieg, *J. Chem. Phys.* **2010**, *132*, 154104.
[37] P. Giacinto, A. Bottoni, M. Calvaresi, F. Zerbetto, *J. Phys. Chem. C* **2014**, *118*, 5032.
[38] Y. Kanai, J. C. Grossman, *Nano Lett.* **2008**, *8*, 908.

Received: December 18, 2014
Revised: January 26, 2015
Published online: February 25, 2015